Journal of The Electrochemical Society, **152** (11) F179-F184 (2005)
0013-4651/2005/152(11)/F179/6/$7.00 © The Electrochemical Society, Inc.

The Effect of the Process Conditions on the Synthesis of Zirconium-Aluminum Oxide Thin Films Prepared by Ultrasonic Spray Pyrolysis

M. Bizarro, J. C. Alonso, and A. Ortiz[z]

Materials Research Institute, National Autonomous University of Mexico, Ciudad Universitaria Coyoacán, D.F. 04510, Mexico

Zirconium-aluminum oxide thin films with different aluminum/zirconium ratios (Al/Zr) have been prepared by ultrasonic spray pyrolysis, using metallic acetylacetonates as source materials. The effect of variations of substrate temperature (T_s), carrier gas flow rate (F_g), and aluminum concentration in the start solution [$(Al/Zr)_s$] on the Al/Zr ratio, the deposition rate (R_d), and refractive index of deposited films is analyzed. The Al/Zr ratio increases when the T_s and [$(Al/Zr)_s$] ratios increase, but it diminishes as F_g is augmented. Moreover, R_d grows when the deposition parameters are incremented. Refractive index acquires values around 1.85 in all cases. X-ray photoelectron spectroscopy results indicate that the Zr 3d and O 1s core levels shift toward low binding energies when aluminum is incorporated. The location of line Al 2p and its symmetry indicates that aluminum atoms are completely oxidized, forming a ternary oxide with zirconium atoms. Infrared transmittance spectra show small absorption bands related with Zr–O and Al–O bonds in a ternary (ZrAlO) oxide. X-ray diffraction spectra show that all the films containing aluminum are amorphous, except that deposited at the highest T_s. In all other studied cases the films are amorphous. The dielectric constant has values between 11.84 and 20.96 depending on the deposition conditions.
© 2005 The Electrochemical Society. [DOI: 10.1149/1.2039607] All rights reserved.

Manuscript submitted March 3, 2005; revised manuscript received June 14, 2005. Available electronically September 8, 2005.

Due to the ultralarge-scale-integration trends, the reduction in the lateral dimensions of devices has, as a consequence, a reduction in the capacitance of metal-oxide-semiconductor (MOS) structures. When a SiO_2 gate dielectric about 1.5 nm thick is required, the leakage current density through the dielectric film can be of the order of a few amperes per square centimeter, which is unacceptable.[1] This fact has originated a great research effort looking for a dielectric material that can replace the silicon dioxide in those devices, keeping the device area small and preventing high leakage current densities. Thicker, high dielectric constant materials films can be used to fulfill these requirements. However, further requirements on the gate dielectric materials are (*i*) the dielectric should be thermodynamically stable on silicon in further processing steps; (*ii*) the gate dielectric should have a large bandgap to achieve a large energy barrier from the conduction band to the Fermi level of the gate electrode to prevent high leakage current densities; (*iii*) sharp interface with the Si substrate to get a low density of interface states.[2] Besides the above requirements, to avoid large leakage current densities through the grain boundaries in crystalline oxides, the dielectric must be of amorphous nature.

Some materials have been suggested to replace the SiO_2 as gate dielectrics, such as Al_2O_3, Ta_2O_5, HfO_2, TiO_2, ZrO_2, etc[3-7] Among them aluminum oxide remains amorphous at very high temperatures, has a large bandgap ($\cong$8.8 eV), but has a relatively low dielectric constant (8–10). Zirconium oxide has a relatively large bandgap ($\cong$6.5 eV) and a high dielectric constant ($\kappa \cong$ 20–30), but it does not remain amorphous at temperatures higher than 500°C. It is known that the amorphous nature of a material can remain at high temperature if another material is mixed with it, in certain chemical concentrations.[8] Insulating thin films for applications in thin-film electroluminescent devices (TFELD) of the MISIM type should have some specific properties, from an electric point of view. During operation of TFELD, the applied voltage is divided between three films so that a larger percentage of that voltage should be applied to the active semiconductor layer. To accomplish this condition, the capacity of insulating films should be as high as possible, which means that the quotient of dielectric constant/ thickness of the film (ε/d) should be high.[9]

Zirconium-aluminum oxide has been proposed as a possible candidate for gate dielectric applications, and also could be applied to TFELD. Thin films of this ternary oxide have been prepared by several methods, such as reactive sputtering, off-axis sputtering, anodization of sputtered-deposited Zr–Al alloys, pulsed laser deposition, and atomic layer chemical vapor deposition.[8,10-13] There are recent reports where the deposition of aluminum oxide and, separately, zirconium oxide thin films, has been carried out by the ultrasonic spray pyrolysis method, at relatively low substrate temperature, using aluminum and zirconium acetylacetonates as source materials, respectively. Aluminum oxide thin films are of amorphous nature for all the substrate temperatures used, and zirconium oxide films are also of amorphous nature for substrate temperatures lower than 500°C. The Al_2O_3 prepared films have a bandgap higher than 6.2 eV, breakdown electric fields of the order of 8 MV/cm, and dielectric constant of 10. Meanwhile, ZrO_2 films have a bandgap of 5.47 eV and breakdown electric fields of the order of 6 MV/cm.[14,15]

The ultrasonic spray pyrolysis method, also called pyrosol, has been well described in several reports. This method is considered as a chemical vapor deposition (CVD) process when the deposited parameters are optimized. It does not require expensive vacuum equipment. It is probably the easiest and lowest cost process to prepare thin films.[16] Zirconium and aluminum acetylacetonates are organometallic compounds that are inexpensive, nontoxic, and stable in air atmosphere at room temperature.

In this work we report the effect of the deposition parameters on the synthesis of zirconium-aluminum oxide films, prepared by the ultrasonic spray pyrolysis method using acetylacetonates as source materials.

Experimental

The zirconium-aluminum oxide films were deposited by the pyrosol process. The start solutions were obtained dissolving zirconium acetylacetonate and aluminum acetylacetonate in pure methanol. It was not necessary, in any case, to add acetic acid to get the complete dissolution of the source materials, since all the solutions were visibly transparent. The following deposition parameters of the pyrosol process were taken into account: substrate temperature (T_s), carrier gas flow rate (F_g), and the $(Al/Zr)_s$ ratio in the start solution. Samples were deposited for different sets of deposition parameters. Case A: The start solution was 0.025 M zirconium acetylacetonate with 5 atom % aluminum acetylacetonate added [$(Al/Zr)_s$ ratio equal to 0.05 in solution]. The carrier gas flow rate (air in the present work) was kept constant at 3.0 l/min. The substrate temperature was varied from 375 up to 525°C, in 25°C steps. Case B: For a start solution similar to that of case A and a constant substrate temperature of 475°C, the carrier gas flow rate took values of 2.0 (AZU18),

[z] E-mail: aortiz@servidor.unam.mx

Downloaded 06 Apr 2010 to 132.248.12.226. Redistribution subject to ECS license or copyright; see http://www.ecsdl.org/terms_use.jsp

2.5 (AZU19), 3.0 (AZU20), and 3.5 (AZU21) l/min. Case C: For a constant substrate temperature of 475°C and a constant carrier gas flow rate of 3.0 L/min, the $(Al/Zr)_s$ ratio in the start solution was varied at 0.0 (AZU1), 0.0125 (AZU2), 0.025 (AZU3), 0.050 (AZU4), 0.075 (AZU5), 0.10 (AZU6), 0.15 (AZU7), 0.20 (AZU8), 0.25(AZU9), and 0.30 (AZU10) values. The substrates used in this work were Pyrex glass slices, Corning 7059 glass slices covered with a transparent conducting layer (TCC), and clear fused quartz slices ultrasonically cleaned with trichloroethylene, acetone, and methanol; and n-type silicon (100) single-crystal slices with 200 Ω cm electrical resistivity. These substrates were chemically cleaned with P etch solution [H_2O (300 mL), HF (15 mL), HNO_3 (10 mL)] in order to remove the native oxide from the surface of the silicon slices. The films deposited onto Pyrex glass were used to measure the thickness; in this case, a small part of the substrate was covered with a cover Pyrex glass to form a step during deposition. The thickness of the deposited films was measured with a Sloan Dektak IIA profilometer. X-ray diffraction spectra were obtained on films deposited onto fused quartz slices with a Siemens D-500 diffractometer using a Cu Kα wavelength (0.154056 nm). In selected preparation conditions the X-ray diffraction spectra were obtained with an integration time of 14 h. The films deposited onto single-crystalline Si slices were used to measure the refractive index (n) and thickness by ellipsometry with a manual Gaertner 117A ellipsometer using the 632 nm line from a He–Ne laser. Infrared transmittance measurements were achieved on these samples with a Fourier transform infrared (FTIR) 205 Nicolet spectrophotometer. In order to obtain the Al/Zr ratio, X-ray photoelectron spectroscopy (XPS) measurements were carried out on films deposited onto c-Si, using an ultrahigh vacuum (UHV) system VG-Scientific Microtech Multilab ESCA2000 with a CLAM4 MCD detector analyzer. The X-ray source used was Mg Kα ($h\nu = 1253.6$ eV) with a 20 mA beam intensity and a polarized anode at 15 kV. The incident X-ray beam was at 55° with respect to the surface normal, and the spectra were acquired with a constant energy step of $E_0 = 20$ eV. The analysis of the spectra was performed using the software SDPv4.1 and the sensitivity factors reported by Scofield. The pressure was maintained constant during the measurements at 1×10^{-8} mbar. The films deposited, at selected preparation conditions, onto Corning 7059 covered with a transparent conductive layer were used to measure the capacitance of Al/ZrAlO/TCC structures, in which the aluminum electrodes were dots, 1.2 mm in diameter, formed by thermal vacuum evaporation through a metallic mask. In the preparation of these MIM structures a small part of the TCC was covered with a cover Pyrex glass during the insulator film deposition to make electrical contact.

Results and Discussion

Case A.— The thickness of the films deposited were obtained by profilometry (on the Pyrex substrate) and by ellipsometry (on the c-Si substrates) measurements. The values obtained by the two techniques were similar for each one of the deposition conditions and take values from 103.4 nm at low T_s to 60 nm at high T_s. From the thickness of the films and deposition time, the deposition rate was calculated. Figure 1 shows the dependence of the deposition rate on the substrate temperature. The deposition rate increases as the substrate temperature increases from 375 to 425°C. For T_s higher than 425°C the deposition rate decreases as T_s increases. This behavior is a common one observed in films deposited by spray pyrolysis. This variation is associated with a better decomposition of the source materials at higher T_s and with des-adsorption of adsorbed species due to the high substrate temperatures. The higher values of R_d for low T_s can be understood as a result of the incorporation of organic radicals in films deposited at low substrate temperatures, because chemical composition measured by XPS indicates that the carbon concentration, associated with the source materials, decreases as T_s increases, from 20 to 8 atom %. The Al/Zr ratio in the deposited films, not shown, varies from values of the order of 0.09, for the lowest temperature, up to 0.32 for highest T_s. For low T_s the oxidation rate of the organic radicals related to source materials has given values, then as T_s increases the decomposition rate of organic radical increases, generating a higher number of metallic radicals, resulting in an increased oxidation rate of these radicals. However, it can be inferred that the oxidation rate of the aluminum radicals is higher than that of the zirconium radicals giving way to higher Al/Zr ratio values. Figure 2 shows that the refractive index of the deposited films is almost independent of T_s. The measured refractive index of films has values around 1.9. All these values are located inside the range of values defined by those obtained for films of Al_2O_3 ($\cong 1.635$)[14] and ZrO_2($\cong 2.1$)[15] deposited by the ultrasonic spray pyrolysis method, although the n values in the present case are closer to the refractive index measured in ZrO_2. Taking into account the variation in the Al/Zr ratio, increasing for high T_s, it could be expected that the n values should go down. These results are ex-

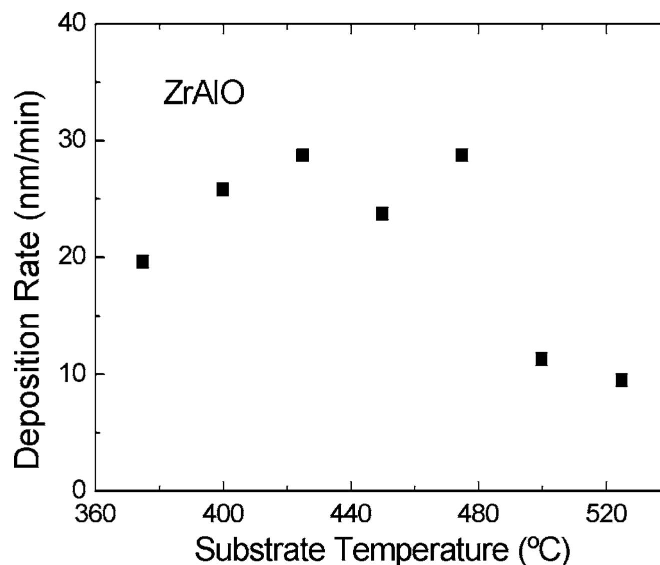

Figure 1. Dependence of the deposition rate on the substrate temperature for zirconium-aluminum oxide, prepared by the pyrosol process. The decreasing trend at high T_s is a typical behavior in films deposited by spray pyrolysis.

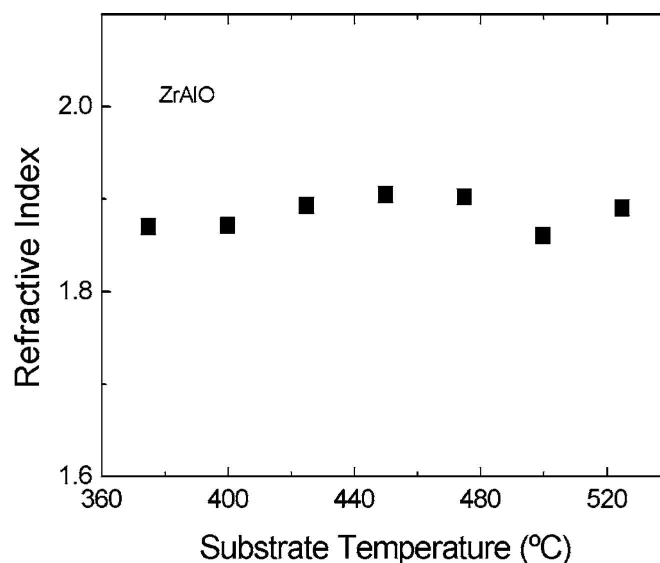

Figure 2. Refractive index as a function of the substrate temperature for Zr–Al–O films. All values are around 1.9.

Downloaded 06 Apr 2010 to 132.248.12.226. Redistribution subject to ECS license or copyright; see http://www.ecsdl.org/terms_use.jsp

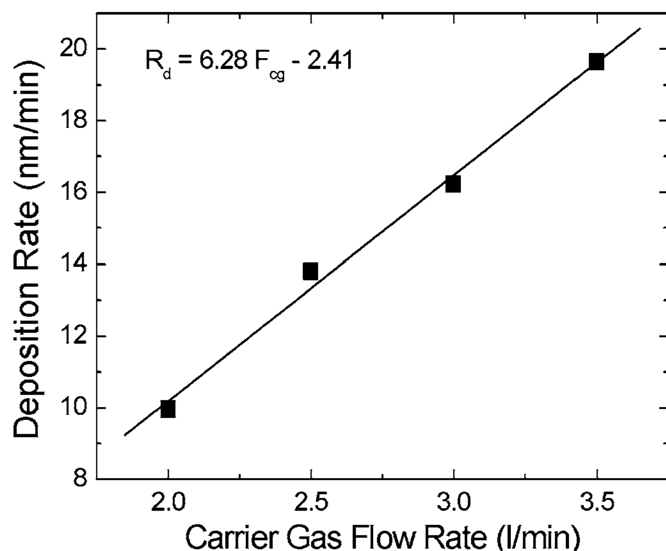

Figure 3. Deposition rate variation as a function of the carrier gas flow rate.

plained considering two possibilities, one associated with the incorporation into the deposited films of high concentrations of organic radicals for low T_s, which does not permit n values close to 2.1. The second possibility is that, for high T_s, the reduction in the incorporation of organic radicals should increase the value of the refractive index, but that reduction is accompanied by an increment in the aluminum incorporation, resulting in a compensation effect where the value of the refractive index is maintained almost constant. A densification effect due to the high T_s is also possible.

Case B.— The variation of the deposition rate as a function of the carrier gas flow rate is shown in Fig. 3; there is an increment in R_d with the increment in F_g. This trend is explained taking into account that the carrier gas flow rate is the parameter that controls the quantity of mass impinging on the surface of the substrate, for constant rate of generation of the small drops of start solution and for a given chemical composition of the start solution. The linear behavior indicates that the decomposition processes of the source materials and the chemical reactions generating the zirconium–aluminum oxide film are of first order, in the range studied. In Fig. 4 it is shown that the Al/Zr ratio as a function of F_g decreases

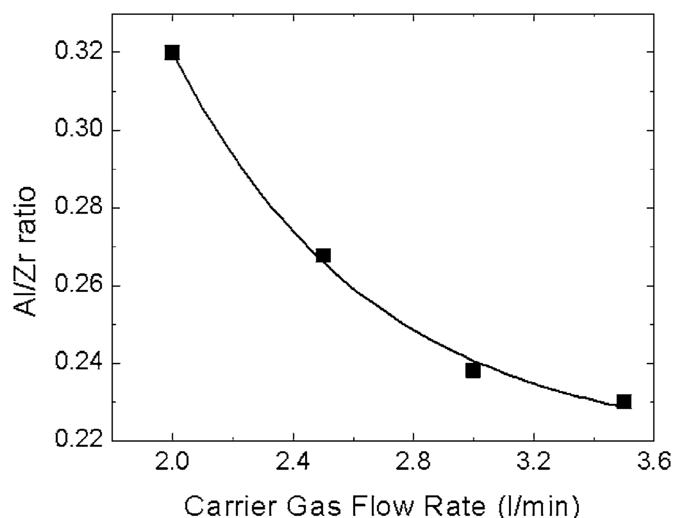

Figure 4. Decreasing exponential variation of the (Al/Zr) ratio for increasing the carrier gas flow rate.

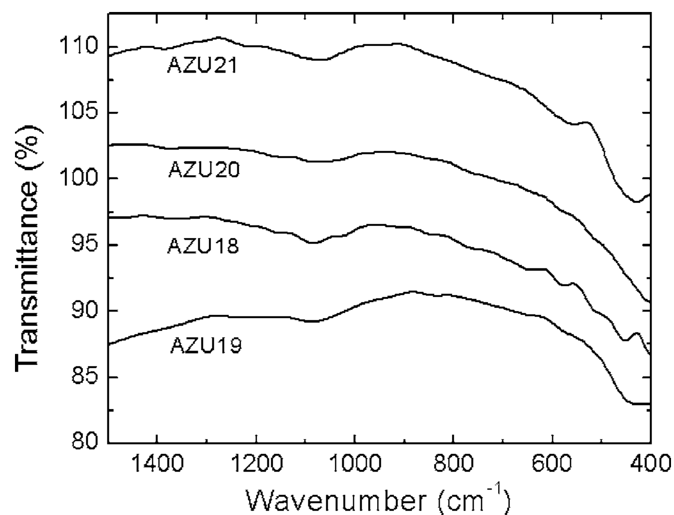

Figure 5. FTIR spectra for zirconium-aluminum oxide films deposited at different carrier gas flow rate. No evidence of vibrations of Zr–O or Al–O bonds is observed.

exponentially. This variation is explained again considering that for low values of F_g the quantity of mass impinging on the substrate is small. In this condition the oxidation rates of radicals related to Zr and Al have given values. However, the Al/Zr ratio has the highest value for the smallest value of F_g, indicating that the oxidation rate by the carrier gas (air) of the aluminum radicals is higher than that of the zirconium radicals. When F_g increases, the Al/Zr ratio decreases; in these conditions more mass impinges on the surface of the substrate. The decreasing trend in the Al/Zr ratio is understood considering that in the start solution the concentration of the zirconium source material is too high in comparison with that of the aluminum source material, and that the oxidation rates of the Al and Zr radicals are constant. Then, the oxidation of aluminum radicals is diminished because there is less time for the oxidation of the aluminum radicals before the next chemical species reaches the surface of the substrate. Given these variations in Al/Zr ratio and in R_d as a function of F_g, it is inferred that the oxidation of the zirconium radicals controls the deposition process, even though the oxidation rate of aluminum radicals is higher than that of zirconium radicals. From ellipsometric measurements it is observed that the refractive index of the deposited films increases from 1.81 up to 1.89 as F_g goes up from 2.0 to 3.5 L/min. This behavior is associated with the variation of the Al/Zr ratio. For higher values of the Al/Zr ratio when the aluminum concentration in deposited films has the highest values, the refractive index acquires its lowest values and, for lower values of the Al/Zr ratio, the zirconium concentration in the material forming the deposited film is high, resulting in higher values of n.

Figure 5 shows the FTIR spectra of films deposited for different values of F_g. In some of these spectra there are small but well-defined absorption bands. The spectrum obtained for the sample with the lowest carrier gas flow rate (AZU18) shows features located at 457 (ZrO_2), 515 (ZrO_2), 582 (Al_2O_3), 649 (ZrO_2,Al_2O_3), and 762 (ZrO_2) cm^{-1}. Some of them can be related to vibration modes of Zr–O and Al–O bonds. However, the location of these bands is near those reported for stoichiometric ZrO_2 and Al_2O_3 compounds.[17,18] The small differences can be explained considering that in the films deposited, in this work, there are Zr–O and Al–O bonds and the simultaneous presence of both kinds of bonds can shift the location of the absorptions bands, indicating that the films are formed by a ternary $Zr_xAl_yO_z$ material. The spectrum of the film deposited with the highest carrier gas flow rate (AZU21) shows two well-defined bands located at 428 and 567 cm^{-1}, which can be associated with vibration modes of Al–O bonds. The location of both is near those reported for stoichiometric Al_2O_3 (alundum).[18] The

Downloaded 06 Apr 2010 to 132.248.12.226. Redistribution subject to ECS license or copyright; see http://www.ecsdl.org/terms_use.jsp

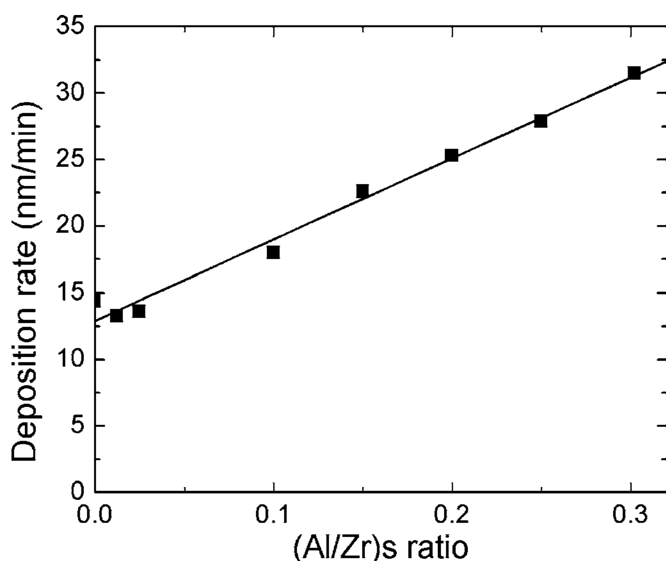

Figure 6. R_d variation as a function of the $(Al/Zr)_s$ ratio. A value of 14 nm/min is related to deposition of a zirconium oxide film.

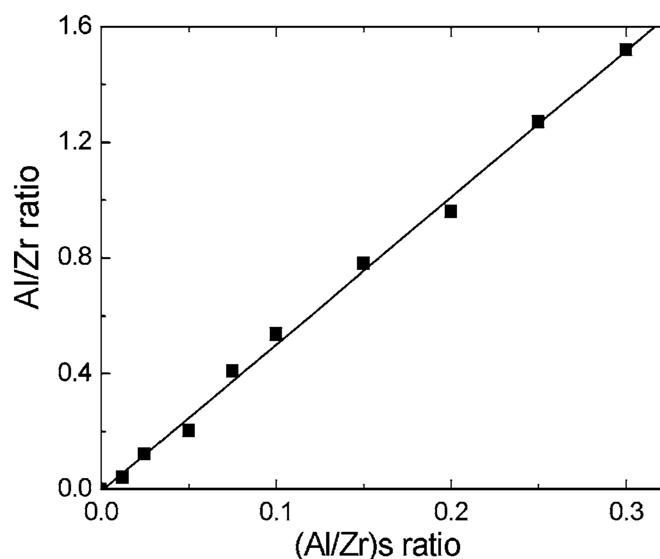

Figure 7. Al/Zr ratio variation as a function of the aluminum quantity added to the start solution. This result indicates a higher aluminum oxidation rate than that of zirconium oxidation.

spectra obtained in samples prepared with medium carrier gas flow rates (AZU19 and AZU20) do not show any well-defined absorption bands that can be related to vibration modes of Zr–O and Al–O bonds. Although the aluminum concentrations in the films are relatively high (Al/Zr ratio values between 0.22 and 0.32), there are not segregates of aluminum or zirconium oxides, given the absence of the broad band of amorphous Al_2O_3[19] and the IR features corresponding to zirconium oxide.[20] All these spectra show well-defined absorption bands located at 1070, 1630, and 3410 cm^{-1}. The band located at 1070 cm^{-1} is related to the stretching vibration mode of silicon dioxide. This silicon dioxide is formed during film deposition as an interface layer between the zirconium-aluminum oxide film and the crystalline silicon substrate.[21] The bands at 3410 and 1630 cm^{-1} are related to the stretching and bending vibrations of O–H groups, respectively. The films probably adsorb water from the atmosphere after deposition. The peak observed around 2350 cm^{-1} is due to carbon dioxide from the air atmosphere present during measurement.

Case C.— Figure 6 shows the dependence of the deposition rate on the aluminum concentration added in the start solution. The deposition rate increases almost linearly with $(Al/Zr)_s$. For this ratio equal to zero, R_d has a value of about 14 nm/min; this is related to zirconium oxide deposition. Although the maximum value of the $(Al/Zr)_s$ ratio is 0.3, solution 0.0325 M of metallic source materials, R_d acquires a value which is double that corresponding to $(Al/Zr)_s = 0$. This appears to indicate that the rate of aluminum oxidation, in air atmosphere, is higher than that of the zirconium oxidation for the substrate temperature used. The refractive index acquires values around 1.85 for all $(Al/Zr)_s$ values. It is unexpected that, even for the highest values of $(Al/Zr)_s$, the refractive index does not show a trend toward the value of refractive index of Al_2O_3 (1.638). It is known that for high deposition rates the density of the deposited films is lower than in those grown with low deposition rates, which is determined by the kinetics of the deposition process. At present, computational simulation studies of the oxidation of the metallic species and film growth processes are being carried out to clarify these results.

In Fig. 7 the dependence of the Al/Zr ratio on the $(Al/Zr)_s$ ratio is shown. This dependence shows an almost linear behavior. However, for a value of $(Al/Zr)_s = 0.3$, the Al/Zr ratio has a value of 1.52, which is higher than that of $(Al/Zr)_s$ by a factor of 5. This appears to indicate once again that the rate of aluminum oxidation is higher than that of zirconium oxidation. However, this fact does not indicate that the rate of zirconium oxidation and zirconium incorporated in the deposited film decreases. The concentration of zirconium source material is constant in the start solution, in all cases, and the number of Zr–O radicals incorporated in the films must be constant. If the rate of aluminum oxidation is higher than that for zirconium, then more Al–O radicals are incorporated in the deposited films, increasing the values of Al/Zr and R_d. The IR spectra for these samples show a similar behavior to that shown in Fig. 5, without clearly defined evidence that could be associated with Al–O or Zr–O bonds associated with separated phases.

Figure 8 shows the normalized photoelectron lines of Al 2p (Fig. 8a), Zr 3d (Fig. 8b), and O 1s (Fig. 8c) core levels, respectively. The spectral lines correspond to the samples prepared with $(Al/Zr)_s$ ratio equal to 0.0 (AZU1), 0.025 (AZU3), 0.075 (AZU5), 0.15 (AZU7), and 0.25 (AZU9). In Fig. 8a it can be observed that the peak related with the core-level Al 2p increases as the $(Al/Zr)_s$ ratio increases; the maximum of the well-defined peaks is located at 74.3 eV. This value and the symmetry of the peak indicate that it corresponds to completely oxidized aluminum (Al^{+3}).[22] However, when Al atoms are incorporated in the zirconium-aluminum oxide compound the location of the core-level Al 2p peak shows a slight shift toward low binding energies in comparison with that reported for aluminum oxide (74.9 eV).[23] The slight shift observed in this case indicates that the aluminum atoms are incorporated in the ternary oxide with zirconium. Meanwhile, the main peak of the Zr 3d core level, in Fig. 8b, shifts from 183.3 eV up to 182.5 eV as the $(Al/Zr)_s$ ratio increases. It has been reported that the location of this spectral peak Zr 3d is 183.44 eV for completely oxidized zirconium.[24] In the present case, the value of 183.3 eV is obtained for the sample without aluminum in the start solution. Then, it can be considered that the film is formed by a stoichiometric zirconium oxide. The doublet Zr 3d is shifted toward lower energies as the aluminum concentration in the deposited film increases. The location of the maximum of the spectral line has a value of 182.5 eV for the sample with higher aluminum concentration. This decreasing binding energy can be due to the generation of Zr–O–Al bonds as more aluminum atoms are incorporated in the films. A similar shift has been observed in zirconium-aluminum oxide annealed films prepared by sputtering.[25] The O 1s core level shows a similar shift, like the Zr 3d core level, toward low binding energies as is shown in Fig. 8c, from 530.6 eV up to 530.0 eV as the $(Al/Zr)_s$ ratio increases. The first value is associated

Downloaded 06 Apr 2010 to 132.248.12.226. Redistribution subject to ECS license or copyright; see http://www.ecsdl.org/terms_use.jsp

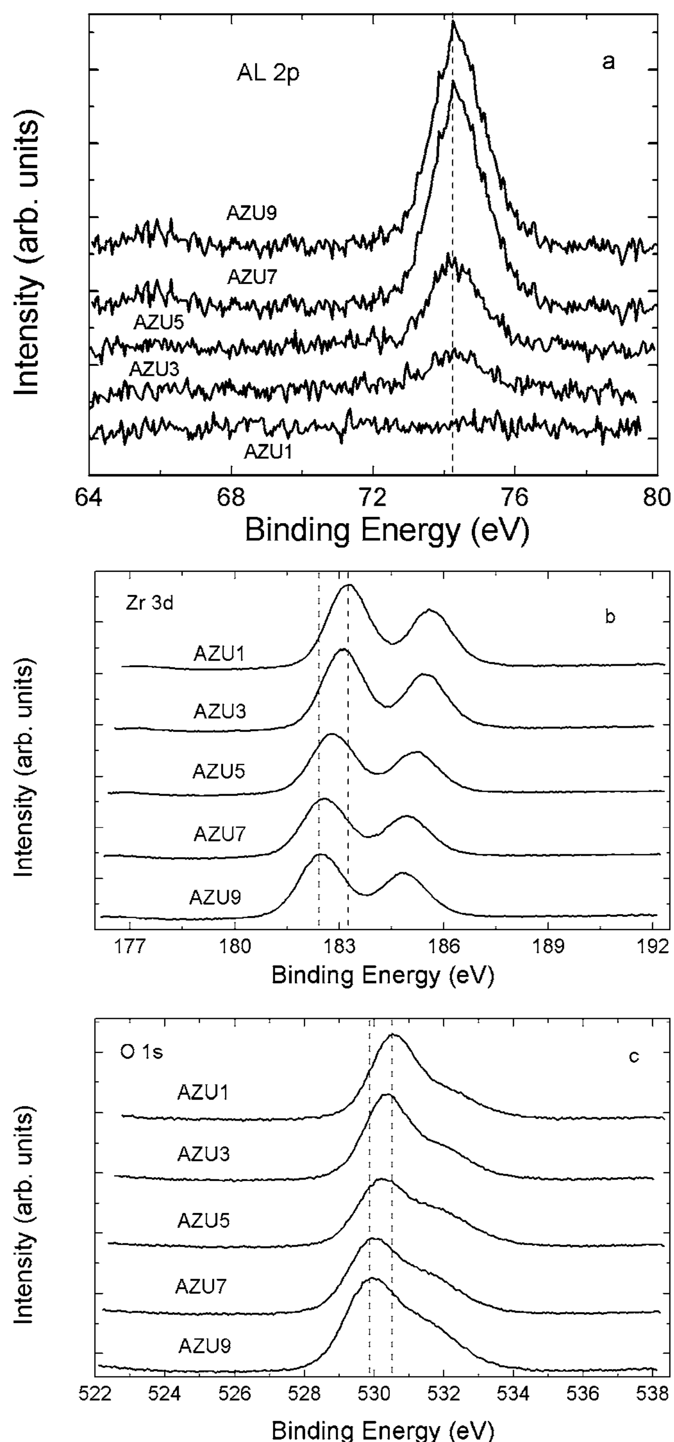

Figure 8. XPS spectra of (a) Al 2p, (b) Zr 3d, and (c) O 1s core levels. The Al 2p peak increases as $(Al/Zr)_s$ increases. Meanwhile, the Zr 3d and the O 1s lines shift toward low binding energies as $(Al/Zr)_s$ increases.

with oxygen forming Zr–O bonds, as is the case for the sample without aluminum in the start solution. For the sample with the highest $(Al/Zr)_s$ ratio value, the location of the peak is shifted toward low binding energies. This slight shift can be due to the generation of Al–O bonds besides the Zr–O bonds. The existence of both of these bonds, Zr–O and Al–O, results in the structure of the spectral line that can be defined by the shoulder on the side of high binding energies. This line is composed of two contributions, one due to Zr–O bonds in the low binding energy region and the other due to Al–O bonds in the high binding energy region, as has been reported earlier.[22] Also, it can be observed that the shoulder on the spectral line increases its magnitude as the $(Al/Zr)_s$ ratio increases; this effect is explained considering that for higher values of the $(Al/Zr)_s$ ratio the concentration of aluminum atoms incorporated in the films is higher, resulting in a higher number of Al–O bonds.

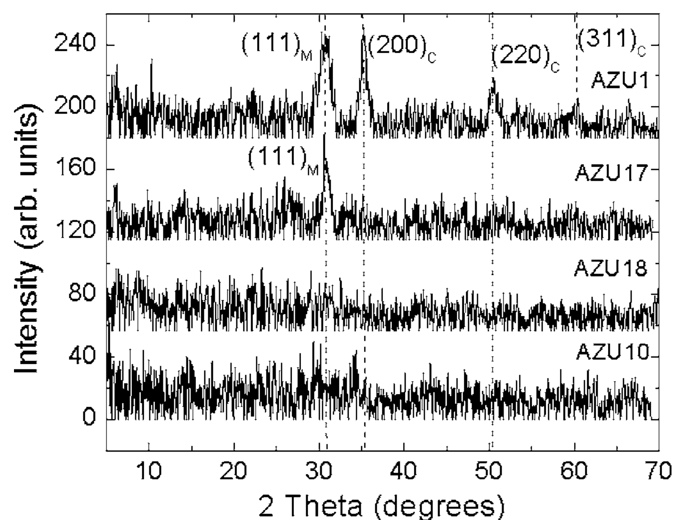

Figure 9. X-ray diffraction spectra for films deposited at selected deposition conditions. The peaks on spectra of samples AZU1 and AZU17 indicate a crystallite size ranging from 10 to 15 nanometers.

Figure 9 shows the X-ray diffraction spectra obtained for samples deposited at selected deposition conditions. The spectrum of the film deposited, as in case C (AZU1), at a substrate temperature of 475°C shows well-defined peaks located at 31.5, 35.3, 50.7, and 60.3°. The peak at 31.5° is associated with reflections in the (111) family planes of the monoclinic phase of ZrO_2.[26] Meanwhile, those located at 35.3, 50.7, and 60.3° are related to reflections in the (200), (220), and (311) planes of the cubic phase of Zr_2O.[27] These peaks have crystallite sizes ranging from 10 up to 15 nanometers, calculated with the formula of Scherrer. The presence of both peaks is explained considering that for this sample the $(Al/Zr)_s$ ratio value is zero, without aluminum added to the spray solution. The substrate temperature has a relatively high value to induce the crystallization of ZrO_2, but it is not high enough to produce the complete oxidation of the metallic zirconium radicals arriving on the surface of the substrate. The spectrum obtained for the film deposited, as in case A (AZU17), at the highest substrate temperature of 525°C shows only the peak located at 31.5°, which is related to the deposition of nanograins of the monoclinic phase of ZrO_2. Although this sample has a relatively high concentration of aluminum atoms incorporated (Al/Zr ratio has a value of 0.32), the substrate temperature is high enough to induce the complete oxidation of zirconium-related radicals and the formation of nanocrystals of ZrO_2. The X-ray diffraction spectra for the films deposited at 475°C, as in case B (AZU18) with the lowest carrier gas flow rate and, as in case C (AZU10), with the highest value of the $(Al/Zr)_s$ ratio, both having higher Al/Zr ratio values, do not show any peak that indicates some crystalline phase of the ZrO_2 and Al_2O_3 compounds. Given the Al/Zr ratio values for these samples, the obtained results in the present case are in agreement with those previously published.[28]

Although the main goal of this work was to analyze the effect of the deposition parameters on the synthesis of ZrAlO compound by ultrasonic spray pyrolysis, the capacitance measurements carried out on the Al/ZrAlO/TCC structures permit us to calculate the dielectric constant values for films deposited at selected deposition conditions.

Downloaded 06 Apr 2010 to 132.248.12.226. Redistribution subject to ECS license or copyright; see http://www.ecsdl.org/terms_use.jsp

Table I. Dielectric constant *k* and Al/Zr ratio values for selected deposition conditions.

Sample	T_s (°C)	F_{gp} (L/min)	F_{gd} (L/min)	$(Al/Zr)_s$ ratio	Al/Zr ratio	*K*
AZU12	400	3.5	1.5	0.05	0.15	20.96
AZU15	475	3.5	1.5	0.05	0.23	13.79
AZU18	475	2.0	1.5	0.05	0.32	16.86
AZU10	475	3.5	1.5	0.30	1.52	11.84

Table I shows the deposition conditions, the values of the Al/Zr ratio obtained from XPS measurements, and the values calculated for the dielectric constant.

The sample prepared at a substrate temperature of 400°C (AZU12) has the highest *k* value for films with aluminum incorporated. It was mentioned above that the Al/Zr ratio increases as T_s increases; then, at low T_s the value of the Al/Zr ratio is relatively low (0.15), indicating that the film deposited has a high Zr–O bond concentration, giving way to the high value of *k*. For higher substrate temperature (AZU15), the value of the Al/Zr ratio increases because more aluminum oxidized related radicals are incorporated in the film, resulting in a decreasing value of the dielectric constant. As shown in Fig. 4, the film prepared with the lowest carrier gas flow rate (AZU18) has values of the Al/Zr ratio as high as 0.32, indicating a high incorporation of Al–O radicals, which should result in a low value of *k*. However, at that value of the carrier gas flow rate it could be a densification effect of the film deposited giving way to a relatively high value of the dielectric constant. The film deposited with the highest value of the $(Al/Zr)_s$ ratio (AZU10) has a relative chemical composition such that the aluminum concentration is higher than that of zirconium by a factor of 1.52. This fact explains the low value of its dielectric constant (11.84) which is closer to that obtained for Al_2O_3 films (10) prepared by spray pyrolysis. Similar results have been obtained in $ZrAlO_x$ deposited by atomic layer CVD.[29] All the *k* values calculated for these films indicate that they are formed by a ZrAlO ternary compound without the existence of separated phases of ZrO_2 and Al_2O_3.

Conclusions

The variations in the Al/Zr ratio values as a function of the deposition parameters indicate that it is possible to control the relative chemical composition of the deposited material by controlling the magnitude of deposition parameters. Refractive index and XPS results show that the deposited material is constituted by a ternary oxide, the metallic atoms being aluminum and zirconium. Similarly, the FTIR results show small bands that can be related to vibration modes of Zr–O and Al–O bonds. They appear to indicate that zirconium-aluminum oxides are the deposited materials. Although the generation of a silicon dioxide interfacial layer is observed, it does not form a crystalline phase of a metallic silicate. X-ray diffraction spectra for samples deposited without aluminum in the start solution and that deposited at the highest substrate temperature indicate the existence of nanocrystals. The materials deposited in all the other deposition conditions are of amorphous nature, even for the lowest aluminum concentration in the films. This result permits us to infer that the amorphous state of zirconium oxide could be stabilized by the aluminum incorporation. Dielectric constant of 20.96 was calculated for films with Al/Zr ratio of the order of 0.15 and a value of *k* of 11.84 is obtained in films with Al/Zr ratio of 1.5.

Acknowledgments

The authors thank J. Fandiño, L. Huerta, S. Jiménez, and L. Baños for technical support.

Instituto de Investigaciones en Materiales assisted in meeting the publication costs of this article.

References

1. A. I. Kingon, J. P. Maria, and S. K. Streiffer, *Nature (London)*, **406**, 1032 (2000).
2. G. D. Wilk, R. M. Wallace, and J. M. Anthony, *J. Appl. Phys.*, **89**, 5243 (2001).
3. P. Ctibor, J. Sedlácek, and K. Nuefuss, *Ceram. Int.*, **29**, 527 (2003).
4. J. L. Autran, R. Devine, C. Chaneliere, and B. Ballaud, *IEEE Electron Device Lett.*, **18**, 447 (1997).
5. B. H. Lee, L. Kang, R. Nieh, W. J. Qi, and J. C. Lee, *Appl. Phys. Lett.*, **76**, 1926 (2000).
6. S. A. Campbell, H. S. Kim, D. C. Gilmer, B. He, T. Ma, and W. L. Gladfelter, *IBM J. Res. Dev.*, **43**, 383 (1999).
7. Y. Z. Hu and S. P. Tay, *J. Vac. Sci. Technol. B*, **19**, 1706 (2001).
8. R. B. van Dover, D. V. Lang, M. L. Green, and L. Manchada, *J. Vac. Sci. Technol. A*, **19**, 2779 (2001).
9. Y. A. Ono, in *Electroluminescence*, Encyclopedia of Applied Physics Vol. 5, p. 295, VCH Publishers, Inc., New York (1993).
10. E. B. O. da Rosa, J. Morais, R. P. Pezzi, L. Miotti, and I. S. R. Baumvol, *J. Electrochem. Soc.*, **148**, G695 (2001).
11. H. Habazaki, K. Takahiro, S. Yamaguchi, K. Shimizu, P. Skeldon, G. E. Thompson, and G. C. Wood, *Philos. Mag. A*, **80**, 1027 (2000).
12. J. Zhu and Z. G. Liu, *Microelectron. Eng.*, **66**, 849 (2003).
13. J. Petry, O. Richard, W. Vadervorst, T. Conard, J. Chen, and V. Cosnier, *J. Vac. Sci. Technol. A*, **21**, 1482 (2003).
14. A. Ortiz and J. C. Alonso, *J. Mater. Sci.: Mater. Electron.*, **13**, 7 (2002).
15. A. Ortiz, J. C. Alonso, and E. Haro-Poniatowski, *J. Electron. Mater.*, **34**, 1 (2005).
16. M. Langlet and J. C. Joubert, in *Chemistry of Advanced Materials, Pyrosol Process or The Pyrolysis of an Ultrasonically Generated Aerosol*, C. N. R. Rao, Editor, p. 55, Blackwell Scientific, Oxford (1993).
17. R. A. Nyquist and R. O. Kagel, in *Infrared Spectra of Inorganic Compounds* (3800-45 cm^{-1}), Vol. 4, The Dow Chemical Company, p. 209–211, Academic Press, Midland, MI (1997).
18. F. F. Bentley, L. D. Smithson, and A. L. Rozek, in *Infrared Spectra and Characteristic Frequencies* ~700-300 cm^{-1}*: A Collection of Spectra, Interpretation and Bibliography*, p. 1564, J. Wiley & Sons, New York (1968).
19. T. Maruyama and S. Arai, *Appl. Phys. Lett.*, **60**, 322 (2002).
20. L. A. Pérez-Maqueda and E. Matijevic, *J. Mater. Res.*, **12**, 3286 (1997).
21. A. Ortiz, J. C. Alonso, V. Pankov, A. Huanosta, and E. Andrade, *Thin Solid Films*, **368**, 74 (2000).
22. M. H. Cho, Y. S. Rho, H. J. Choi, S. W. Nam, D. H. Ko, J. H. Ku, H. C. Kang, D. Y. Noh, C. N. Whang, and J. Jeong, *J. Vac. Sci. Technol. A*, **20**, 865 (2002).
23. O. Renault, L. G. Gosset, D. Rouchon, and A. Ermolirff, *J. Vac. Sci. Technol. A*, **20**, 1867 (2002).
24. S. K. Dey, C. G. Wang, D. Tang, M. J. Kim, R. W. Carpenter, C. Werkhoven, and E. Shero, *J. Appl. Phys.*, **93**, 4144 (2003).
25. M. J. Guittet, J. P. Crocombetle, and M. Gautier-Soyer, *Phys. Rev. B*, **63**, 125117 (2001).
26. JCPDS File Card no. 37-1484.
27. JCPDS File Card no. 65-0461.
28. C. Zhao, O. Richard, E. Young, H. Bender, G. Roebben, S. Haukka, S. De Gendt, M. Houssa, R. Carter, W. Tsai, O. Van Der Biest, and M. Heyns, *J. Non-Cryst. Solids*, **303**, 144 (2002).
29. W. F. A. Besling, E. Young, T. Conard, C. Zhao, R. Carter, W. Vandervorst, M. Caymax, S. De Gent, M. Heyns, J. Maes, M. Touminen, and Savi Haukka, *J. Non-Cryst. Solids*, **303**, 123 (2002).

Downloaded 06 Apr 2010 to 132.248.12.226. Redistribution subject to ECS license or copyright; see http://www.ecsdl.org/terms_use.jsp